PHARMACEUTICAL NANOTECHNOLOGY

Polyelectrolyte Stabilized Drug Nanoparticles via Flash Nanoprecipitation: A Model Study With β-Carotene

ZHENGXI ZHU,[1] KATRIN MARGULIS-GOSHEN,[2] SHLOMO MAGDASSI,[2] YESHAYAHU TALMON,[3] CHRISTOPHER W. MACOSKO[1]

[1]Department of Chemical Engineering and Materials Science, University of Minnesota, Minneapolis, Minnesota 55455

[2]Institute of Chemistry, Casali Institute of Applied Chemistry, Hebrew University of Jerusalem, Jerusalem 91904, Israel

[3]Department of Chemical Engineering, Technion-Israel Institute of Technology, Haifa 32000, Israel

Received 19 September 2009; revised 19 December 2009; accepted 23 December 2009

Published online 8 February 2010 in Wiley Online Library (wileyonlinelibrary.com). DOI 10.1002/jps.22090

ABSTRACT: Polyelectrolyte protected β-carotene nanoparticles (nanosuspensions) with average diameter of <100 nm were achieved by turbulent mixing and flash nanoprecipitation (FNP). Three types of multi-amine functional polyelectrolytes, ε-polylysine (ε-PL), poly(ethylene imine) (PEI), and chitosan, were investigated to electrosterically protect the nanoparticles. Particle size and distribution were measured by dynamic light scattering (DLS); particles were imaged via scanning electron microscopy (SEM) and cryogenic transmission electron microscopy (cryo-TEM). Low pH and high polyelectrolyte molecular weight gave the smallest and most stable particles. High drug loading capacity, >80 wt%, was achieved by using either PEI or chitosan. X-ray diffraction (XRD) patterns showed that β-carotene nanoparticles were amorphous. These findings open the way for utilization of FNP for preparation of nanoparticles with enhanced bioavailability for highly water insoluble drugs. © 2010 Wiley-Liss, Inc. and the American Pharmacists Association J Pharm Sci 99:4295–4306, 2010

Keywords: nanoparticles; polymeric drug delivery systems; mixing; polyelectrolytes; formulation; nanosuspensions; biodegradable polymers; stabilization; supersaturation; light-scattering

INTRODUCTION

Drug solubility enhancement is one of the most important challenges in the field of pharmaceutics. Nearly 40% of all new pharmacologically potent compounds exhibit poor aqueous solubility. This leads to their low effective concentration in biofluids and therefore poor bioavailability.[1,2] Those compounds must be either chemically altered or pharmaceutically prepared into their final dosage forms in order to enhance their solubility prior to administration as medicines. One way to enhance the aqueous solubility is to reduce the size of drug particles to the nanometric range. The Kelvin equation[3,4] predicts that reducing the size of a spherical particle will increase its saturation solubility. Moreover, drug dissolution rate will increase inversely with particle radius as described by the Noyes–Whitney equation.[4] Thus, by drastically reducing particle size, both the saturation solubility and especially the dissolution rate can be improved.[4–7] Another great advantage of nanometer scale particles is in drug delivery. The leaky vasculature of tumors permits passive targeting of cancer therapy agents. Such passive targeting, known as the enhanced permeation and retention (EPR) effect, is possible for drug particles at a size of about 100 nm.[8]

Several methods are used for preparing nanoparticles (nanosuspensions) of poorly soluble organic therapeutically active molecules.[9,10] Those methods include wet/dry milling,[1,11] supercritical solution expansion,[12,13] spray freezing into liquid,[14] preparation from confined structures such as micro/nanoemulsions,[15–18] and controlled precipitation from solution.[5,19–21] A novel precipitation method, flash nanoprecipitation (FNP) was presented recently for preparation of suspensions of nanoparticles.[22–27]

In the FNP technique, a highly hydrophobic drug is dissolved along with a block copolymer in a water

Correspondence to: Christopher W. Macosko (Telephone: 1-612-625-0092; Fax: 1-612-626-1686; E-mail: macosko@umn.edu)

Journal of Pharmaceutical Sciences, Vol. 99, 4295–4306 (2010)

miscible organic solvent. This solution is injected into a small chamber at a high velocity along with water. The high velocity generates turbulent mixing, causing the hydrophobic drug and polymer to precipitate very rapidly, forming nanometer scale particles. The block copolymer is amphiphilic: typically a hydrophilic poly(ethylene glycol) (PEG) block covalently bonded to a hydrophobic block. The hydrophobic block precipitates with the drug, arresting particle growth while the pendant PEG blocks stabilize the particles against aggregation. PEG blocks can be tipped with ligands to target specific cells.[28] FNP also permits combining several hydrophobic drugs and incorporation of imaging agents.[29] FNP is a relatively fast and simple process which can be readily scaled up to larger volume production.

Up to now only amphiphilic block copolymers have been used, either premade[22–27,30–32] or *in situ* formed by rapid coupling reactions during mixing.[33] This study shows that polyelectrolytes which are dissolved in the aqueous phase can also stabilize nanoparticles via FNP. When amphiphilic block copolymers are used for FNP they co-precipitate with the hydrophobic drug. Thus, particle cores can be a mixture of the polymer and drug.[33] Water soluble polyelectrolytes do not provide extra supersaturation during precipitation, and are expected to only adsorb on the particle surface. Comparing nanoparticles stabilized with both methods can give insight into the mechanisms and kinetics of the nanoparticle formation via FNP, which occur at the nanometer scale and evolve from microseconds to milliseconds.

The mechanism for stabilization is also different between block copolymers and polyelectrolytes. The water soluble block in a block copolymer gives steric stabilization. Polyelectrolytes can give both steric and electrostatic stabilization. The charge along polyelectrolyte chains can build a strong double layer around the particle and, if the polyelectrolyte adsorbs loosely, polymer loops and chain ends will extend from the particle surface providing a steric shield (see Fig. 1c).[34]

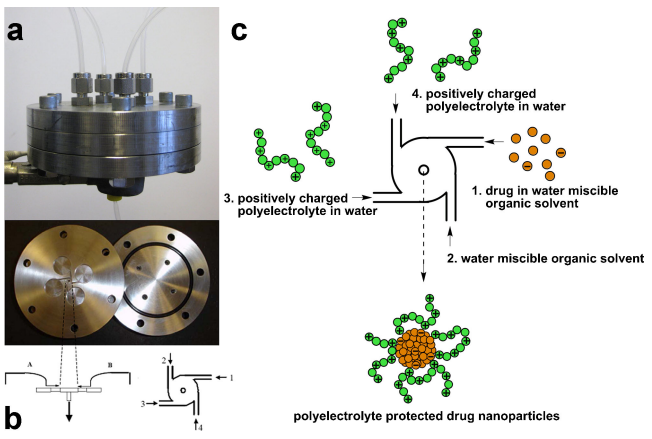

Figure 1. Vortex mixer: (a) assembled, (b) section with schematic of flow path, and (c) schematic of particle formation.

Also, crystallinity of the nanoparticles formed via FNP will be studied in the first time. With polyelectrolytes the effect of stabilizer on drug crystallization is removed because the water soluble polymer does not precipitate with the drug. Finally polyelectrolytes are attractive from the viewpoint of pharmaceutical manufacture. The use of water soluble polyelectrolytes decreases the usage of organic solvents. In this study, three different polyelectrolytes are chosen: ε-polylysine (ε-PL), poly(ethylene imine) (PEI), and chitosan (see Scheme 1).

ε-PL is a naturally occurring poly(amino acid), which has been used as a food additive and generally recognized as safe (GRAS) by FDA. It is biodegradable, biocompatible, and of low cytotoxicity. It is considered to be nontoxic in acute, subchronic, and chronic feeding studies in rats and nonmutagenic in bacterial reversion assays.[35–38]

PEI is a cationic polymer exhibiting high charge density in an acidic aqueous solution. It has been widely used as a precipitant for proteins or nucleic acids to make complexes, which can transfect proteins or genes through cell walls.[39,40] The most commonly used form is branched PEI which has a globular shape and a ratio of 1/2/1 of primary/secondary/tertiary amines. Branched PEI is synthesized by a cationic ring-opening polymerization from aziridine.[41] The high degree of branching comes from the easy proton transfer from the tertiary aziridinium ion to other amino groups, which are activated during chain propagation. In contrast to branched PEI, linear PEI only contains secondary amines, and is usually synthesized by polycondensation of *N*-(2-aminoethyl)-aziridine in aqueous medium or cationic isomerization of ring-opening polymerization of 2-oxazolines, followed by hydrolysis of the resultant polyamide.[42,43]

Chitosan is a cationic polyelectrolyte, a β-(1-4)-linked copolymer of 2-amino-2-deoxy-β-D-glucan (GlcN) and 2-acetamido-2-deoxy-β-D-glucan (GlcNAc), obtained by a heterogeneous deacetylation of chitin which is a naturally abundant polysaccharide and a major exoskeleton component of crustaceans and insects.[44,45] Like other polycations, chitosan does have potential cytotoxicity.[46] However, chitosan exhibits biocompatibility, low toxicity, and low immunogenicity following intravenous and oral administration to animal models.[45] It is readily biodegraded by several human enzymes, such as lysozyme. It is inexpensive and approved as a safe dietary supplement.[44] The properties of chitosan include the ability to adhere to mucosal layers, due to the electrostatic interaction with negatively charged sialic acid residues in mucin.[47] This makes chitosan especially useful for poorly water soluble drug delivery and targeting.

 DOI 10.1002/jps

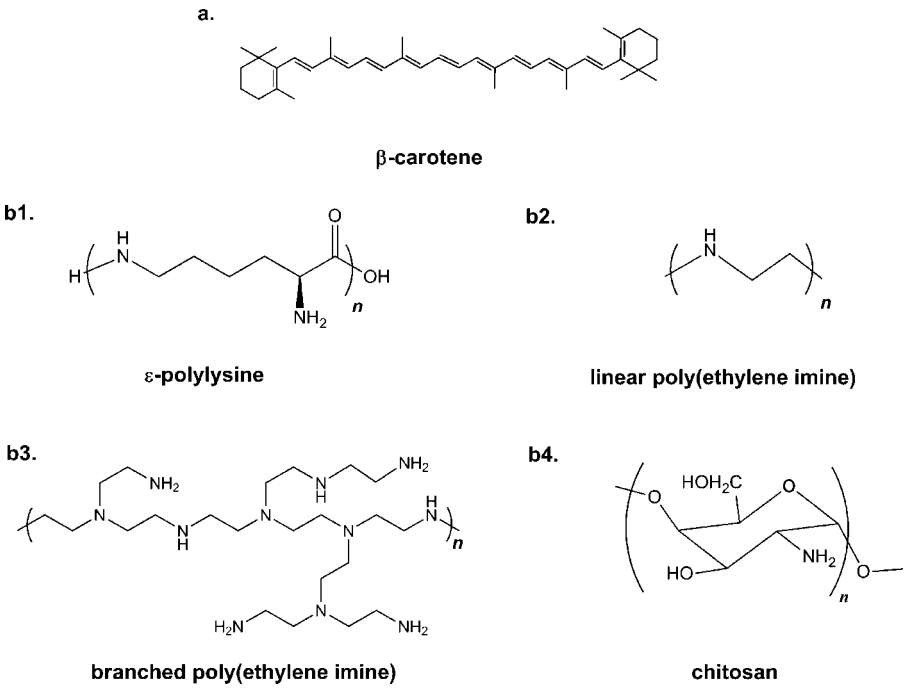

Scheme 1. Chemical structures of (a) β-carotene, and (b1–b4) polyelectrolytes.

Chitosan is also GRAS by FDA. In this study, chitosan was particularly successful, forming stable and amorphous particles of 60 nm with a drug loading capacity of >80%.

As a model drug we chose β-carotene, a precursor of vitamin A and listed in the U.S. National Cancer Institute drug dictionary. It is highly insoluble in water ($\log P = 15.5$, ACD model from www.emolecules.com) while soluble in tetrahydrofuran (THF). The extremely low solubility was confirmed by high performance liquid chromatography (HPLC) (see β-Carotene Nanoparticles Section). β-Carotene can serve as a model for valuable drugs which are water insoluble but soluble in a water miscible solvent, such as THF, acetone, acetonitrile, methanol, or ethanol. Drug examples include statin cholesterol regulators, such as lovastatin and simvastatin; antifungal substances such as itraconazole;[32] benzodiazepine tranquilizers, such as diazepam; lipid regulatory agents, such as fenofibrate; chemotherapy agents, such as paclitaxel,[31] and docetaxel; immune system modulators, such as tacrolimus and cyclosporine A.

MATERIALS AND METHODS

Materials

β-Carotene (≥97%), water (HPLC grade) and tetrahydrofuran (THF, HPLC grade) were purchased from Aldrich, USA and used as received.

Microbial ε-PL (4000 g mol^{-1}, notated as 4k in this paper; 50 wt% water solution) was received from the Chisso Co., Japan Linear PEI (25,000 g mol^{-1}, notated as 25k) and two branched versions (10,000 and 1,800 g · mol^{-1}, notated as 10 and 1.8k) were purchased from Alfa Aesar and another branched PEI (60,000 g · mol^{-1}, notated as 60k; 50 wt% water solution) was purchased from Aldrich. Low molecular weight chitosan (degree of deacetylation 90%, 50,000 g · mol^{-1}, notated as 50k) and medium molecular weight chitosan (degree of deacetylation 85%, 250,000 g · mol^{-1}, notated as 250k) were purchased from Aldrich.

Particle Preparation

Our vortex mixer and the FNP process are illustrated in Figure 1. Typically two of the mixer inlets were connected to two gas-tight plastic syringes (60 mL, Kendall Monojet) via Teflon tubing, 1.6 mm of inner diameter. Each plastic syringe contained 45 mL of polyelectrolyte water solution, and was driven by an infusion syringe pump (Harvard Apparatus, model 945). The other two inlets were connected to two gas-tight glass syringes (10 mL, SGE) via Teflon tubing. One of the syringes contained 5 mL of a 1% β-carotene THF solution while the other contained 5 mL of pure THF. The two glass syringes were driven by a second infusion syringe pump (Harvard Apparatus, PHD 2000 programmable). The pumps propelled the four streams at high velocities into the small mix chamber, generating high turbulence. Complete dimensions and evaluation of mixing performance using competitive reactions with small molecules were given by Liu et al.[23] For most of the experiments, the flow rates were 120 mL/min for the plastic syringes and 13.3 mL/min for the glass syringes. From these flow rates we

calculate a mean Reynolds number (Re) $\approx$ 18,000, using the relation (Eq. 1) reported by Liu et al.[23]:

$$Re = \sum_{i=1}^{4} Re_i = \frac{\rho D}{s} \sum_{i=1}^{4} \frac{Q_i}{\eta_i} \quad (1)$$

where ρ is the density of the mixture (assuming $1.0 \times 10^3\,\mathrm{kg \cdot m^{-3}}$ at room temperature); D is the chamber diameter ($6.0 \times 10^{-3}\,\mathrm{m}$); s is the cross-sectional area of the inlet nozzles ($1.65 \times 10^{-6}\,\mathrm{m^2}$); Q_i is the flow rate of the ith component; η_i is the viscosity of the ith component (0.89 mPa · s unless stated otherwise). Note that to compare Re between mixers such as the confined impinging jets it may be better to use a characteristic size of the inlet nozzles rather than D, the chamber diameter.[22,24,25] The outlet of the mixer was connected via Teflon tubing to a beaker, where the nanoparticle suspensions were collected. The total injection time was about 23 s.

Characterization

All samples were analyzed in the mixed liquid, water with 10% of THF, and also with 1 wt% of NaCl added to this THF/water solution. Salt was used to test the electrostatic stability of the particles; 1 wt% was chosen because it is similar to the ion concentration in body fluids. Particle size and distribution were determined by dynamic light scattering (DLS) using a ZetaPALS (Brookhaven Instruments, diode laser BI-DPSS wavelength of 659 nm, round cuvette). The light intensity correlation function was collected at 25°C and a scattering angle of 90°. The correlation function is a combination of the diffusion coefficient, D_i, of each particle which is converted into particle diameter, d_i, with the Stokes–Einstein equation (Eq. 2),

$$d_i = \frac{k_b T}{3\pi\eta D_i} \quad (2)$$

where k_b is the Boltzmann constant. Correlation functions were downloaded from the ZetaPALS and fit using the REPES model. REPES yields a series of discrete particle diameters to represent the particle size distribution. We have found it more accurate than the cumulant model used in most commercial instruments. The software, GENDIST, was used to solve the REPES algorithm,[48,49] and provided the size in an intensity distribution. The intensity averaged particle size, $\overline{d}_I$, is defined in Eq. 3,

$$\overline{d}_I = \frac{\sum n_i d_i^6}{\sum n_i d_i^5} \quad (3)$$

where n_i is the number of particles with a diameter of d_i. The mass averaged diameter, $\overline{d}_m$, is more practically useful than the usual intensity average for estimating drug loading and availability. It is defined in Eq. 4,

$$\overline{d}_m = \frac{\sum n_i m_i d_i}{\sum n_i m_i} = \frac{\sum n_i d_i^4}{\sum n_i d_i^3} \quad (4)$$

where m_i is the mass of a particle with a diameter of d_i.

When a large amount of the polyelectrolyte was used, there was a significant amount of the free polymer in the aqueous medium of the final suspension. This increases the viscosity of the medium, which must be accounted for in Eq. 2 to obtain the correct particle diameter. Viscosities were measured with an AR-G2 rheometer (TA Instruments) using 40 mm diameter parallel-plates. All samples showed Newtonian behavior over the shear rate range of 1–200 $\mathrm{s^{-1}}$. For the ε-PL solutions the viscosity was the same as water, 0.890 mPa · s, and for the PEI solutions $\eta \leq 0.96$ mPa · s, thus no correction was made. However, due to the high molecular weight of the chitosan, these samples showed a large increase in viscosity as illustrated in Figure 2. When 1 wt% of sodium chloride was added, there was significantly less increase, in agreement with the observations by Cho et al.[50]

An electrode (model SR-259) with a square cell was used with the ZetaPALS for zeta potential (ζ) measurements. Smoluchowski's model[3] was used for the samples in 1 wt% of saline, and Huckel's model[3] for the samples without saline. The viscosities were corrected for the chitosan concentrations.

To test the reproducibility of the mixing and subsequent DLS and zeta potential measurements, four individual runs were performed by mixing 1 wt% of β-carotene THF solution with water at Re of 18,000. The measurements gave $\overline{d}_m \pm \sigma = 85 \pm 7$nm and $\zeta = -19.2 \pm 3.4$ mV. Another three individual batches of PEI protected β-carotene gave $\overline{d}_m \pm \sigma = 82 \pm 5$nm

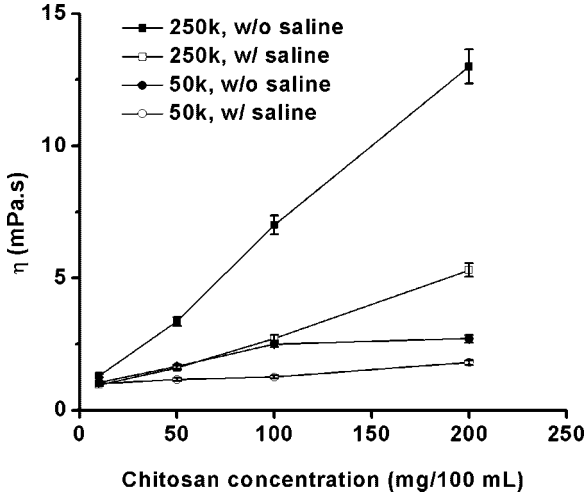

Figure 2. Viscosity versus chitosan concentration in 90 mL of deionized water and 10 mL of THF, without or with 1 wt% saline.

 DOI 10.1002/jps

and $\zeta = +68.5 \pm 3.8$ mV. Thus, systematic errors including both reproducibility of mixing and property measurements were within ±10% for $\overline{d}_m$ and within ±4 mV for ζ.

Cryogenic transmission electron microscopy (cryo-TEM) specimens were prepared in a controlled environment vitrification system (CEVS) maintained at 30°C and 100% relative humidity. They were vitrified in liquid ethane at its freezing point, and transferred into an FEI T12 G^2 TEM by a Gatan 626 cryo-holder and its "work-station."[51] Images of the specimens, kept at about −170°C, were recorded at 120 kV acceleration voltage by a Gatan US1000 cooled CCD camera.

To prepare samples for scanning electron microscopy (SEM) a glass Pasteur pipette was first filled with a small amount of the suspension, and then emptied, leaving minute amounts of liquid on the inner wall. This nanosuspension was then aspirated onto a silica wafer that had been washed with HPLC grade THF and water. After evaporation at room temperature, the sample was sputter coated with a 30 Å layer of Pt and imaged with a JEOL 6500 SEM.

HPLC was used to measure the concentration of the encapsulated β-carotene in the nanoparticles and the free β-carotene in THF and water mixture. The β-carotene nanoparticles were removed from 0.5 mL of the suspension using a centrifugal filter (YM-100, Microcon) with a membrane cut-off of 100 kDa (8 nm pore size) under 12,000*g*. The filtrate was freeze dried. Then 0.2 mL of THF was used to redisolve the β-carotene to get a higher concentration. The filtered nanoparticles were freeze dried, and extracted by 5 mL of methanol/THF (4/1) with stirring overnight. The carrier solvent was acetonitrile/methanol/THF (20/70/10) eluted through a C18 RP (Beckman) HPLC column at a flow rate of 1 mL/min. The injection volume was 20 μL. β-Carotene was detected by UV–Vis detector (Beckman 168) at the wavelength of 470 nm. The drug loading capacity (C_{DL} %) is defined as the ratio of the mass of the drug trapped in the nanoparticles to the total mass of the nanoparticles.

X-ray diffraction (XRD) patterns of the nanoparticles were collected using a Bruker-AXS micro-diffractometer with a 2.2 kW sealed Cu X-ray source. Powder samples of nanoparticles were prepared via centrifugal filtration. The wet powders were measured 4 h after the mixing.

RESULTS AND DISCUSSION

Mixing and Mixing Rate

Higher mixing velocities lead to better homogeneity of supersaturation, giving a more uniform nucleation rate. This uniformity results in smaller particles with narrower size distribution.[52] Moreover, faster mixing provides a higher density of energy dissipation, which increases the kinetic energy of nanoparticles. During mixing, particle aggregation is inhibited to some degree by the kinetic energy of the particles.

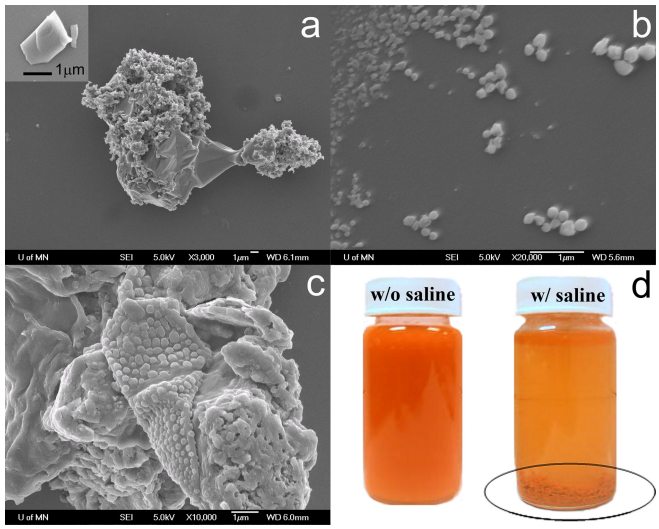

Figure 3. SEM images of β-carotene particles made by (a) simple stirring, (b) FNP, (c) FNP followed by addition of 1 wt% saline, and (d) photos of (b) and (c). The inset in (a) is the as received powder of β-carotene.

Figure 3a shows β-carotene particles made by simple stirring. They are much bigger and broader in distribution than those made by FNP via vortex mixing, Figure 3b. The micron sized aggregates in Figure 3a are composed of smaller particles, and smooth plate-like regions. These plate-like regions indicate crystallinity by comparison with the highly crystalline raw powder (the inset image and Fig. 11). Compared with FNP, a stirred tank produces much less intense mixing and THF requires longer time to diffuse away to the aqueous phase. During this time period, the particles are still swollen with THF and sticky. They therefore have more chance to aggregate and even coalesce, and β-carotene has more time to reorient to enable crystallization. Moreover, high speed stirring only produces low energy dissipation, 10^{-1}–10^{2} W · kg^{-1}, while in FNP the confined turbulent jet mixing with high flow rates dissipates 10^{4}–10^{5} W · kg^{-1}.[22,53] This high energy dissipation inhibits particle aggregation when the particles are still sticky, allowing more solvent to diffuse out of the nanoparticles before possible aggregation. Thus, the particles are harder and remain separated from each other after mixing.

In order to know the flow rate required for producing sufficient mixing, we measured mass averaged diameters of particles produced at several *Re*'s. As shown in Figure 4, at *Re* greater than about 3,000, the mass averaged diameter approached an asymptotic value around 90 nm. Liu[27] reported a

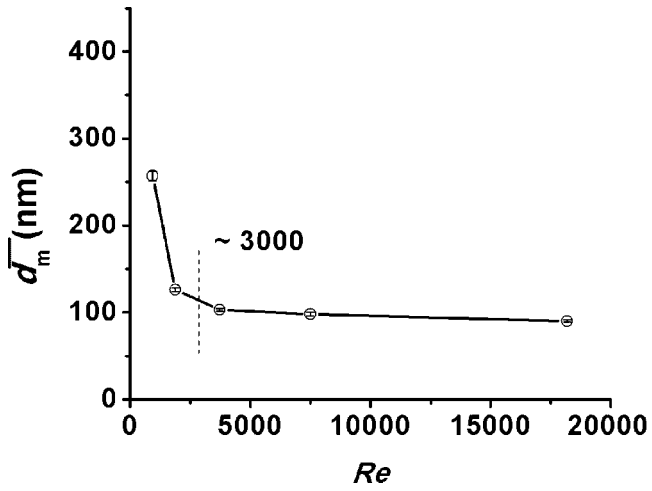

Figure 4. Mass averaged diameter of β-carotene nanoparticles versus Reynolds number (*Re*). The error bars represent the standard deviations of the DLS measurements ($n = 4$). Systematic errors in $\overline{d}_m$, including both reproducibility of mixing and DLS measurements, are within ±10% as shown in Characterization Section. *Re* calculation is based on the chamber diameter as described in Particle Preparation Section and Eq. 1.

critical *Re* of 2,000 for polystyrene-*b*-poly(ethylene glycol) protected β-carotene nanoparticles with a vortex mixer of the same dimensions. The polystyrene hydrophobic block may have provided extra supersaturation during FNP. Liu's particles were larger, indicating incorporation of PS-*b*-PEG block copolymer into the β-carotene nanoparticles.

For all mixing with either ε-PL or PEI, $Re \approx 18{,}000$ was chosen hereinafter. For the mixing with chitosan, the flow rates were the same. However, as shown in Figure 2, the viscosity of the chitosan/water solutions was significantly increased, which reduced *Re* to ~6,000 for the 50k chitosan and ~1,200 for the 250k at the highest investigated concentrations.

β-Carotene Nanoparticles

Due to the low solubility of β-carotene in water, nanoparticles could be produced by FNP (Fig. 3b and 4). However, without any polyelectrolyte they were unstable. Particle size doubled within 4 h and all the particles sedimented on the bottom with the colorless supernatant within one day. The particles have a slightly negative surface charge ($\zeta \approx -20$ mV; see Tab. 1–3), and when 1 wt% of NaCl was added they precipitated immediately (Fig. 3c and d). The negative surface charge may come from impurities or oxidation.[54] It is generally considered that if $-30\text{ mV} \le \zeta \le +30\text{ mV}$, the surface charge alone is not sufficient to stabilize nanoparticles for a long time period.[3]

The mass of dissolved β-carotene in the suspending medium was determined by HPLC. Only 3.1×10^{-4} mg of β-carotene was found in the solution after 50 mg was vortex mixed into 10 mL of THF and 90 mL of H_2O, that is, 99.999% of the β-carotene precipitated (supersaturation ratio 1.6×10^5). This low solubility (3.1 ng/mL) ensures that the β-carotene nanoparticles are relatively stable in terms of recrystallization and Ostwald ripening, which was also observed by Liu et al.[30] This extremely low solubility will result in a very slow release rate, therefore the drug release profile was not investigated in this study.

ε-PL Protected β-Carotene Nanoparticles

Since the β-carotene nanoparticles were unstable especially in saline, a stabilizer must be added. Because β-carotene nanoparticles were slightly negatively charged (see Tab. 1), a positively charged polyelectrolyte was expected to adsorb on the surface of the nanoparticles, acting potentially as both an electrostatic and steric stabilizer to prevent aggregation. A natural and water-soluble polyelectrolyte, ε-PL, was initially chosen.

The protonation degree of the amine groups of ε-PL ($pK_a \approx 9.0$)[55,56] was adjusted with concentrated HCl from a naturally basic condition (pH 8.5), to neutral, and acidic (pH 4). With ε-PL at pH 8.5, its protonation degree was expected to be very slightly, and ζ of the β-carotene nanoparticles increased from −20 to −8 mV (Tab. 1). The nanoparticles aggregated both with and without saline, because of either a low amount of adsorbed polyelectrolyte or smaller ζ. Without saline, this smaller ζ even induced particles to aggregate faster (Fig. 6) than β-carotene alone which doubled the size in 4 h. At pH 7 and 4, ζ's increased to about +50 mV (see Tab. 1), the particles

Table 1. Stability of ε-PL protected β-carotene nanoparticles at different pH in 90 mL of H_2O and 10 mL of THF

β-carotene (mg)	50		50		50		50	
pH of ε-PL	7		8.5		7		4	
ε-PL (mg)	0		50		50		50	
1 wt% saline	w/o	w/	w/o	w/	w/o	w/	w/o	w/
$\overline{d_m}$ (nm)[a]	89	—	—	—	180	—	148	—
Zeta potential (mV)[a]	−19.9	−0.1	−7.8	−2.0	+52.3	—	+49.6	+8.1
Stable (Y/N)	N	N	N	N	Y	N	Y	N

[a]Systematic errors including mixing are within ±10% for $\overline{d_m}$ and within ±4 mV for ζ as shown in Characterization Section.

Table 2. Stability of branched PEI (60K) protected β-carotene at different pH in 90 mL of H_2O and 10 mL of THF

β-carotene (mg)	50		50		50		50		50	
pH of Branched PEI	9		7		4		7		7	
Branched PEI (mg)	50		50		50		0		50	
	Add branched PEI during mixing						—		Add afterward	
1 wt% saline	w/o	w/	w/o	w/	w/o	w/	w/o	w/	w/o	w/
$\overline{d_m}$ (nm)[a]	50	261	77	99	90	102	92	> 1000	89	102
Zeta potential (mV)[a]	+41.2	+2.3	+71.1	+21.5	+67.6	+30.6	−23.5	−0.1	+66.4	+18.4
Stable (Y/N)	Y	N	Y	Y	Y	Y	N	N	Y	Y

[a]Systematic errors including mixing are within ±10% for $\overline{d_m}$ and within ±4 mV for ζ as shown in Characterization Section.

were <200 nm by DLS, with no visible sedimentation up to 6 weeks without saline. However, in 1 wt% of saline, the particles sedimented rapidly, in a few minutes to a few days. Figure 5 shows typical cryo-TEM and SEM images without saline. The size distribution by DLS indicates that there may be a bimodal population.

The amount of ε-PL adsorbed on the surface may be low due to low charge density of the chain. Increasing the concentration of ε-PL may compensate the effect of this low charge per chain. To test this, more ε-PL was added and diameter measured versus time (Fig. 6). With the feed ratio of β-carotene/ε-PL = 1/5, at even pH 8.5 the nanoparticles were stable for at least 1 week in saline and 7 weeks without saline.

PEI Protected β-Carotene Nanoparticles

Linear PEI has a higher density of amino groups than ε-PL (compare b1 and b2 in Scheme 1) and its molecular weight is also higher, 25k versus 4k. However, at 50 mg and pH 7 it stabilized β-carotene particles only marginally better than ε-PL at pH 8.5. Aggregates were observed from the SEM image as well (Fig. 7d). Branched PEI was much more effective, even at 10k. The 60 and 10k branched PEIs (Fig. 7a and b) produced individual, fairly spherical particles, which did not sediment for a few weeks. Significant aggregation occurred in the case of the very low molecular weight branched PEI, 1.8k (Fig. 7c), and the particles sedimented quickly after saline was added. This instability is probably due to its low molecular weight. The 1.8k PEI was too short to build a barrier for steric stabilization. The reason that the 25k linear PEI is less stable than the 10k branched PEI is less clear. The linear PEI is expected to lay down flatter onto the surface of the β-carotene nanoparticles than the globular-like branched PEI. Thus, the branched PEI chains will have longer effective steric spacers than the linear PEI, and have more effective steric stability.

In order to explore the maximum drug loading capacity (C_{DL} %) of β-carotene, lower concentrations of PEI (60k) were used to stabilize the suspension at pH 7. As shown in Figure 8b, nanoparticles stabilized with 10 mg PEI showed very slow increase in the size over 4 weeks, either with or without saline. However, a very low concentration of PEI, 2.5 mg, only stabilized nanoparticles about 1 day in saline (not shown). Thus, from the ratio, β-carotene/(β-carotene + PEI) = 50/(50+10) = 0.83, the drug loading capacity (C_{DL} %) is at least 83% at pH 7.

Figure 8 also shows the effect of pH. Without adding saline, the nanoparticles were stable at all investigated pH for at least 5 weeks, because ζ's were much higher than +30 mV (see Tab. 2) and the nanoparticles were able to be stabilized by the high surface charges. The pK_a of the primary amine of PEI

Table 3. Stability of chitosan protected β-carotene nanoparticles at pH 4 in 90 mL of H_2O and 10 mL of THF

β-carotene (mg)	50		50		50		50	
Chitosan (mg)	50 Low M. W. (50 k)		50 Medium M. W. (250 k)		0		50 Medium M. W. (250 k)	
	Add chitosan during mixing				—		Add afterward	
1 wt% saline	w/o	w/	w/o	w/	w/o	w/	w/o	w/
$\overline{d_m}$ (nm)[a]	60	97	55	55	+83	>1000	79	80
Zeta potential (mV)[a]	+37	+28	+38	+26	−17	−0.1	—	+29
Stable (Y/N)	Y	Y	Y	Y	N	N	Y	Y

[a]Systematic errors including mixing are within ±10% for $\overline{d_m}$ and within ±4 mV for ζ as shown in Characterization Section.

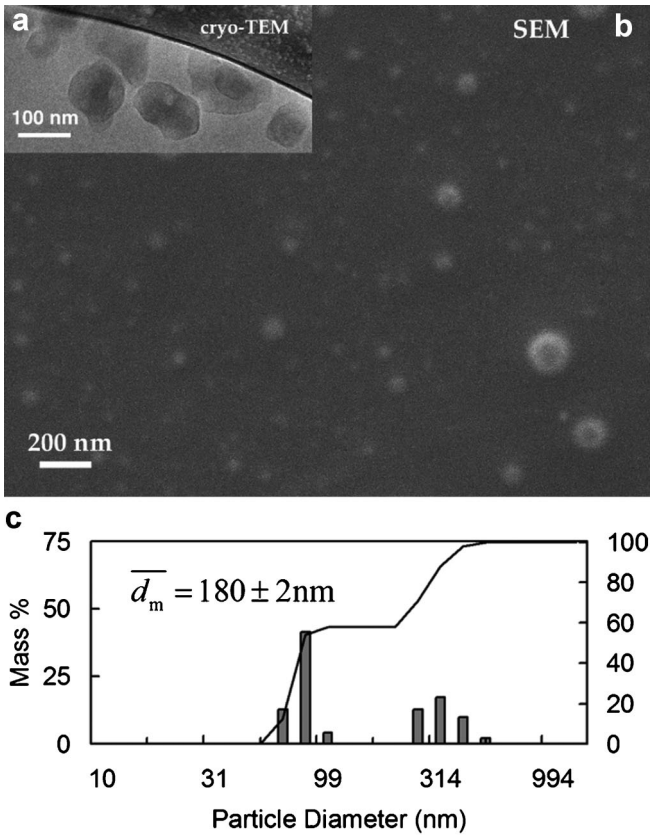

Figure 5. (a) Cryo-TEM image, (b) SEM image, and (c) particle size distribution by DLS of β-carotene (50 mg) nanoparticles protected by ε-PL (50 mg) at pH 7 without saline. The discrete values of diameter in the size distribution are the result of REPES fitting.

is about 9.5.[57,58] The protonation degrees of PEI chains at pH 9, 7, and 4 are 10%, 30%, and 65%, respectively.[59] After adding saline, the positive charges on PEI chains were neutralized in some degree,

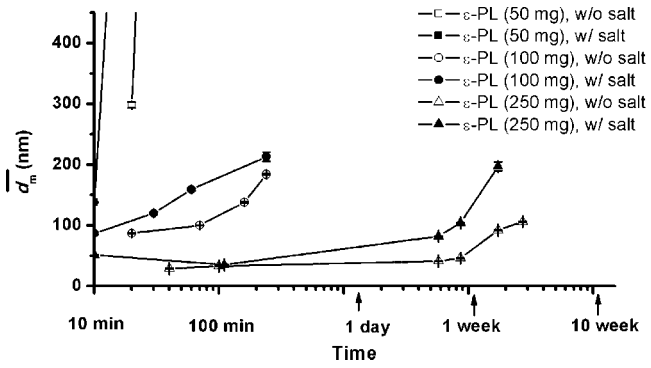

Figure 6. Stability (mass averaged particle diameter vs. time) of β-carotene (50 mg) nanoparticles protected by ε-PL in different concentration with or without 1 wt% saline at pH 8.5. The error bars represent the standard deviations of the DLS measurements ($n = 4$). Samples with 50 mg of ε-PL sedimented within half an hour. $\overline{d}_m$ was much higher than 1 μm and not shown on this plot.

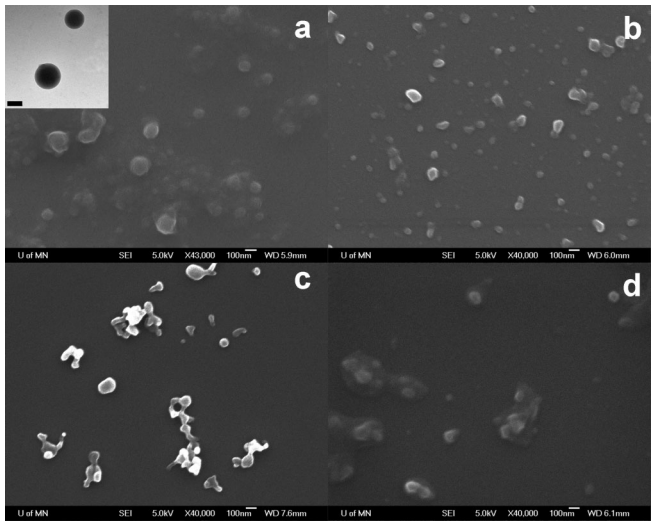

Figure 7. SEM images showing the effect of PEI (50 mg) molecular weight on β-carotene (50 mg) nanoparticles at pH 7: (a) branched PEI (60k) (inset cryo-TEM), (b) branched PEI (10k), (c) branched PEI (1.8k), and (d) linear PEI (25k) (all scale bars are 100 nm).

and ζ's in all cases decreased significantly (see Tab. 2). Assuming that ζ is equal to surface charge, DLVO theory[3] predicts that particles with small surface charge of ≤30 mV and 1% salt will have no electrostatic energy barrier and thus should aggregate. However, at pH 7 and 4, the nanoparticles stayed under 200 nm for at least the 5 weeks investigated. This stability with small positive surface charge indicated that the nanoparticles were stabilized by

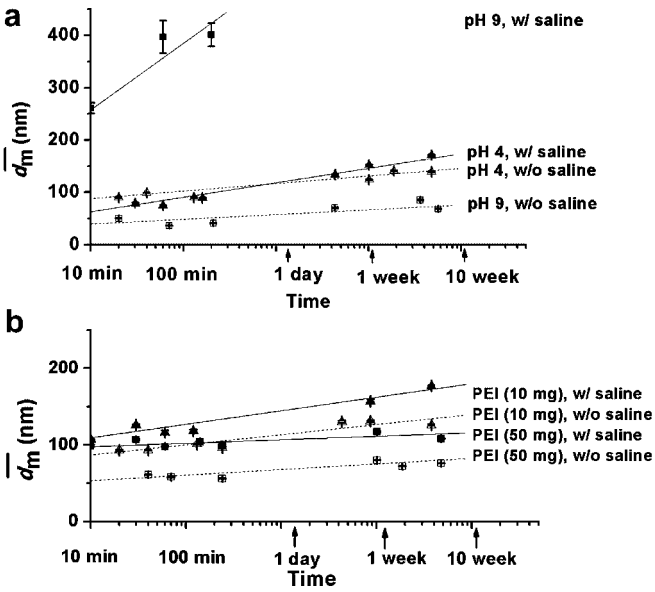

Figure 8. Stability of branched PEI (60k) (50 mg) protected β-carotene (50 mg) nanoparticles with or without 1 wt% saline (a) at pH 4 and 9, (b) at pH 7 with different concentration of PEI. The error bars represent the standard deviations of the DLS measurements ($n = 4$).

DOI 10.1002/jps

steric repulsion. The positive charges on the PEI chains were not sufficiently neutralized, and PEI chains were still able to adsorb on the β-carotene nanoparticles. As well, the PEI protected nanoparticles showed positive ζ's around 20–30 mV. At pH 9 with salt, the particle size increased quickly, and the suspensions were not stable, which indicated that the β-carotene nanoparticles lacked both electrostatic and steric stabilization. This makes sense. At pH 9 the protonation degree was only 10%. Due to being shielded by the salt, the positive charges on the PEI chains appeared much lower. Little PEI was able to adsorbed on the particle surface. As well, surface charges of the β-carotene nanoparticles were neutralized by the salt. Thus, ζ showed a value very close to zero (see Tab. 2) and the β-carotene nanoparticles aggregated.

Chitosan Protected β-Carotene Nanoparticles

Two different molecular weight chitosan (50 and 250 $kg\,mol^{-1}$) were used as the polyelectrolyte. Because chitosan is water insoluble under neutral or basic conditions, only acidic solutions (pH 4) were chosen for the experiments. The pK_a of the amino groups in chitosan is about 6.5,[60] and at pH 4 it is positively charged. Compared with ε-PL and PEI, the chosen chitosan has longer linear chains, and thus much higher viscosity than water, especially in the high concentrations. As mentioned in Characterization Section, this increase in viscosity was accounted for in the DLS and ζ measurements and *Re* determination.

With the feed ratio of β-carotene/chitosan = 50 mg/50 mg, as shown in SEM images in Figure 9a and b, nanoparticles seemed dispersed better by 250k than 50k chitosan. Although $\overline{d}_m$ was around 60 nm for both without saline, it appears from the size distributions that the primary particles are smaller, and there is a small population of aggregates >200 nm, which could be removed by filtration if necessary.

After saline was added (see Tab. 3), $\overline{d}_m$ increased more with the 50k than with the 250k chitosan, although ζ's were very close to each other with the two different chitosan samples. Higher molecular weight appears to give greater capability of steric stabilization.

To explore the maximum C_{DL} %, different mass concentrations of chitosan varying from 10 to 200 mg in 100 mL were used to stabilize 50 mg of β-carotene at pH 4. As shown in Figure 10, with 10 mg of chitosan, generally the particle sizes were a little greater than other cases either in saline or without saline. While, with 50, 100, 200 mg of the polyelectrolyte, the particle sizes were similar to each other. After adding saline, the particle sizes increased more in the 10 mg case than in other cases. The increase of

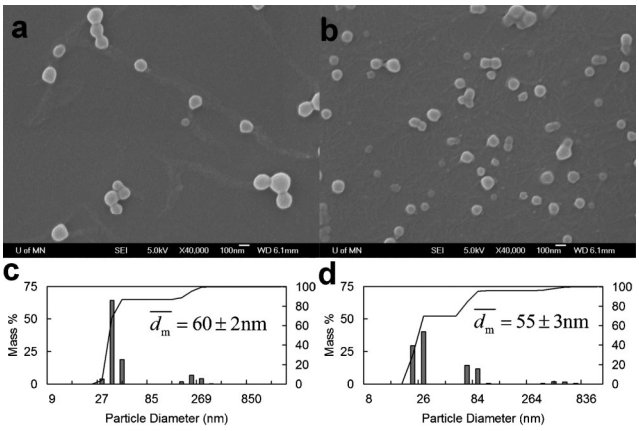

Figure 9. SEM images of β-carotene nanoparticles protected by (a) 50k and (b) 250k chitosan, and particle size distributions by DLS for (c) 50k and (d) 250k. All are at pH 4 with 50 mg β-carotene/50 mg chitosan. The discrete values of diameter in the size distribution are the result of REPES fitting.

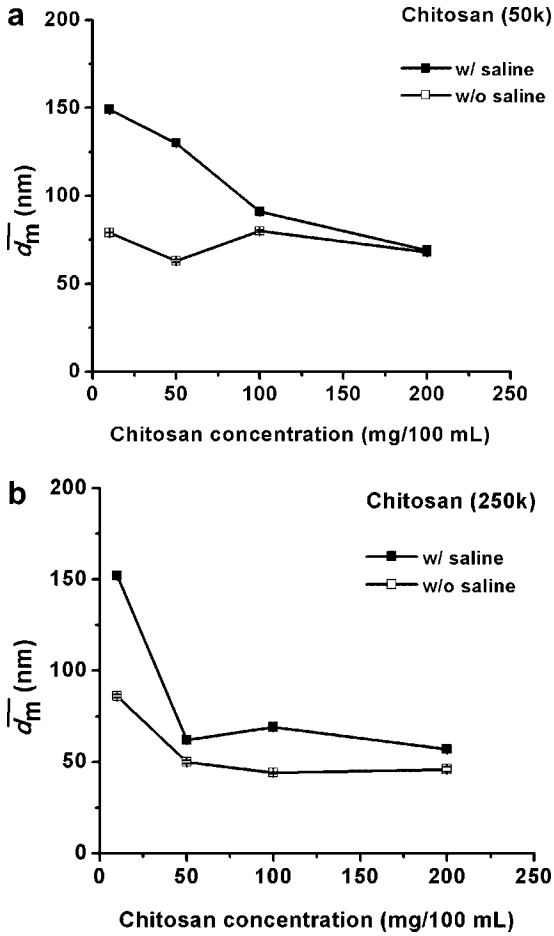

Figure 10. Mass averaged particle size versus concentration of chitosan (a) 50k and (b) 250k at pH 4 after 3–5 h. The error bars are smaller than the standard deviations of the DLS measurements ($n = 4$). Systematic errors including mixing which is within ±10% as shown in Characterization Section.

the sizes came from the slight aggregation of the particles. However, in all cases even with 10 mg of chitosan in saline, the particle sizes still remained below 200 nm for at least 1 week. Therefore, based on the feed ratio of 50 mg of β-carotene/10 mg of chitosan, $C_{DL}\% \geq 83\%$. This value is in agreement with $C_{DL}\%$ of 89.9 wt% from HPLC measurements on particles made with 50 mg of β-carotene/50 mg of 50k chitosan. In this sample, about 45 mg of chitosan molecules is nonadsorbed and in a free state in the aqueous medium. This indicates that our chitosan stabilized particles contain 90% of β-carotene.

To further study the mechanism and kinetics of polymer stabilization in FNP we added the polyelectrolyte half a minute after particle formation. The stream of β-carotene particles from the vortex mixer was poured into a solution of polyelectrolyte such that the final composition was the same as that when all components were injected into the vortex mixer. The last entry in Tab. 2 shows that adding the 60k PEI immediately after formation also gave stable but slightly larger particles than those produced by simultaneous precipitation with PEI. Adding the 250k chitosan after forming the particles also stabilized them, but their size was significantly larger, 80 nm versus 55 nm. Chitosan adsorbs so fast that it slowed β-carotene particle growth or aggregation.

CRYSTALLINITY OF NANOPARTICLES

Bioavailability of drugs is related with the crystallinity of nanoparticles which affects their dissolution.[61] Thus, the particle powders were characterized by XRD as shown in Figure 11. All nanoparticles made by FNP showed diffuse diffraction patterns, and therefore were in the amorphous state, whether the stabilizing polyelectrolytes were added or not. However, the purchased β-carotene powder showed several sharp XRD peaks and was highly crystalline. Auweter et al.[62] reported that β-carotene particles in the 100–200 nm size range exhibited some crystallinity. They produced their particles by precipitation from an alcohol solution with water and gelatin as a stabilizer. The highly amorphous state of our nanoparticles resulted from very fast precipitation, ~20 ms[26]. The THF diffused so rapidly into the water phase that the large β-carotene molecules did not have enough time to align and pack tightly.

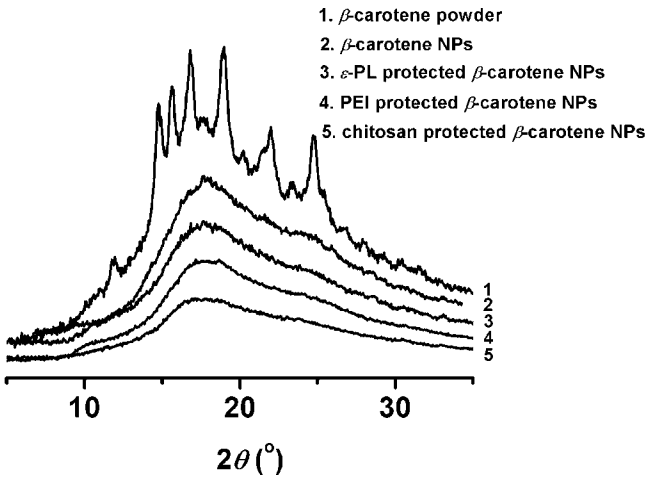

Figure 11. XRD patterns of (1) β-carotene powder, (2) β-carotene nanoparticles (NPs), and β-carotene protected by (3) ε-PL, (4) branched PEI (60k), and (5) chitosan (250k).

CONCLUSIONS

For the first time polyelectrolytes, rather than amphiphilic block copolymers, were used to stabilize particles formed by FNP. Spherical β-carotene nanoparticles with an average diameter <100 nm and very high loading, 80–90 wt%, were produced using either branched PEI (polyethylene imine) or chitosan. Higher molecular weight polyelectrolytes had a better stabilizing effect than the lower ones, yielding the nanoparticles as small as 60 nm. The polyelectrolytes in an acidic or neutral pH were more effective than those in a basic solution. Zeta potential (ζ) measurements demonstrated that the polyelectrolytes provided both electrostatic and steric stabilization. We believe that these amino functional, positively charged polyelectrolytes adsorbed onto the surface of the β-carotene nanoparticles due to their hydrophobic surface and slight negative charge. The fact that smaller size particles were produced when the polyelectrolyte/water solutions were mixed simultaneously with β-carotene/THF rather than mixed sequentially indicates that especially chitosan adsorbs extremely rapidly, at a rate comparable to the precipitation of β-carotene.

The β-carotene nanoparticles precipitated so fast that they were in the amorphous state, independent on the nature of the stabilization. Amorphous drug nanoparticles are expected to have a higher bioavailability in vivo. These results with β-carotene as a model hydrophobic drug, show that FNP could be applied to a variety of highly hydrophobic drugs which have solubility properties similar to β-carotene. Moreover, chitosan is very attractive for producing nanoparticles for oral delivery due to its biocompatibility, cost and approval for use in food supplementary.

ACKNOWLEDGMENTS

We thank Yutaka Miura at the University of Tokyo for characterizing ε-PL, Udaya Toti for HPLC measurement, Wei Fan for assisting in XRD measure-

ment, Thomas Hoye and Jayanth Panyam for fruitful discussions, Michael Tsapatsis for the access of DLS apparatus, and Chisso Corporation for providing ε-PL. This work was supported by the National Science Foundation under the NIRT Program (Award Number CTS-0506966), IPRIME at the University of Minnesota, MRSEC at the University of Minnesota, and the Lady Davis Fellowship Foundation at the Technion. Parts of this work were carried out in the University of Minnesota, Institute of Technology Characterization Facility, which receives partial support from NSF through the NNIN program.

REFERENCES

1. Bushrab FN, Müller RH. 2003. Nanocrystals of poorly soluble drugs for oral administration. J New Drugs 5:20–22.
2. Lipinski CA. 2002. Poor aqueous solubility – An industry wide problem in drug discovery. Am Pharm Rev 5:82–85.
3. Hiemenz PC, Rajagopalan R. 1997. Principles of colloid and surface chemistry, 3rd edition. New York: Marcel Dekker Inc.
4. Muller RH, Jacobs C, Kayser O. 2001. Nanosuspensions as particulate drug formulations in therapy Rationale for development and what we can expect for the future. Adv Drug Deliv Rev 47:3–19.
5. Matteucci ME, Brettmann BK, Rogers TL, Elder EJ, Williams RO, Johnston KP. 2007. Design of potent amorphous drug nanoparticles for rapid generation of highly supersaturated media. Mol Pharm 4:782–793.
6. Horn D. 1989. Preparation and characterization of microdisperse bioavailable carotenoid hydrosols. Angew Makromol Chem 166:139–153.
7. Horn D, Rieger J. 2001. Organic nanoparticles in the aqueous phase - theory, experiment, and use. Angew Chem Int Ed 40:4331–4361.
8. Haag R, Kratz F. 2006. Polymer therapeutics: Concepts and applications. Angew Chem Int Ed 45:1198–1215.
9. Wang G, Uludag H. 2008. Recent developments in nanoparticle-based drug delivery and targeting systems with emphasis on protein-based nanoparticles. Expert Opin Drug Deliv 5:499–515.
10. Hu JH, Johnston KP, Williams RO. 2004. Nanoparticle engineering processes for enhancing the dissolution rates of poorly water soluble drugs. Drug Dev Ind Pharm 30:233–245.
11. Merisko-Liversidge E, Liversidge GG, Cooper ER. 2003. Nanosizing: A formulation approach for poorly-water-soluble compounds. Eur J Pharm Sci 18:113–120.
12. Perrut A, Jung J, Leboeuf F. 2005. Enhancement of dissolution rate of poorly-soluble active ingredients by supercritical fluid processes. Part I: Micronization of neat particles. Int J Pharm 288:3–10.
13. Turk M, Hils P, Helfgen B, Schaber K, Martin HJ, Wahl MA. 2002. Micronization of pharmaceutical substances by the Rapid Expansion of Supercritical Solutions (RESS): A promising method to improve bioavailability of poorly soluble pharmaceutical agents. J Supercrit Fluids 22:75–84.
14. Hu JH, Johnston KP, Williams RO. 2004. Rapid dissolving high potency danazol powders produced by spray freezing into liquid process. Int J Pharm 271:145–154.
15. Margulis-Goshen K, Magdassi S. 2009. Formation of simvastatin nanoparticles from microemulsion. Nanomedicine: NBM 5:274–281.
16. Desgouilles S, Vauthier C, Bazile D, Vacus J, Grossiord JL, Veillard M, Couvreur P. 2003. The design of nanoparticles obtained by solvent evaporation: A comprehensive study. Langmuir 19:9504–9510.
17. Kamishny A, Magdassi S. 2007. Nanoparticles in confined structures: Formation and application. In: Tadros TH, editor. Colloid stability: The role of surface force, 1st edition. Weinheim: Wiley-VCH. pp 207–234.
18. Shekunov BY, Chattopadhyay P, Seitzinger J, Huff R. 2006. Nanoparticles of poorly water-soluble drugs prepared by supercritical fluid extraction of emulsions. Pharm Res 23: 196–204.
19. Chen JF, Zhang JY, Shen ZG, Zhong J, Yun J. 2006. Preparation and characterization of amorphous cefuroxime axetil drug nanoparticles with novel technology: High-gravity antisolvent precipitation. Ind Eng Chem Res 45:8723–8727.
20. Chen XX, Young TJ, Sarkari M, Williams RO, Johnston KP. 2002. Preparation of cyclosporine A nanoparticles by evaporative precipitation into aqueous solution. Int J Pharm 242: 3–14.
21. Rogers TL, Gillespie IB, Hitt JE, Fransen KL, Crowl CA, Tucker CJ, Kupperblatt GB, Becker JN, Wilson DL, Todd C, Elder EJ. 2004. Development and characterization of a scalable controlled precipitation process to enhance the dissolution of poorly water-soluble drugs. Pharm Res 21:2048–2057.
22. Johnson BK. 2003. Flash nanoprecipitation of organic actives via confined micromixing and block copolymer stabilization. Ph.D. Dissertation, Department of Chemical Engineering, Princeton University, Princeton.
23. Liu Y, Cheng CY, Prud'homme RK, Fox RO. 2008. Mixing in a multi-inlet vortex mixer (MIVM) for flash nano-precipitation. Chem Eng Sci 63:2829–2842.
24. Johnson BK, Prud'homme RK. 2003. Chemical processing and micromixing in confined impinging jets. AICHE J 49:2264–2282.
25. Johnson BK, Prud'homme RK. 2003. Flash NanoPrecipitation of organic actives and block copolymers using a confined impinging jets mixer. Aust J Chem 56:1021–1024.
26. Johnson BK, Prud'homme RK. 2003. Mechanism for rapid self-assembly of block copolymer nanoparticles. Phys Rev Lett 91:1183021–1183024.
27. Liu Y. 2007. Formulation nanoparticles by flash nanoprecipitation for drug delivery and sustained release. Ph.D. Dissertation, Department of Chemical Engineering, Princeton University, Princeton.
28. Gindy ME, Ji SX, Hoye TR, Panagiotopoulos AZ, Prud'homme RK. 2008. Preparation of poly(ethylene glycol) protected nanoparticles with variable bioconjugate ligand density. Biomacromolecules 9:2705–2711.
29. Gindy ME, Panagiotopoulos AZ, Prud'homme RK. 2008. Composite block copolymer stabilized nanoparticles: Simultaneous encapsulation of organic actives and inorganic nanostructures. Langmuir 24:83–90.
30. Liu Y, Kathan K, Saad W, Prud'homme RK. 2007. Ostwald ripening of beta-carotene nanoparticles. Phys Rev Lett 98: 0361021–0361024.
31. Ansell SM, Johnstone SA, Tardi PG, Lo L, Xie SW, Shu Y, Harasym TO, Harasym NL, Williams L, Bermudes D, Liboiron BD, Saad W, Prud'homme RK, Mayer LD. 2008. Modulating the therapeutic activity of nanoparticle delivered paclitaxel by manipulating the hydrophobicity of prodrug conjugates. J Med Chem 51:3288–3296.
32. Kumar V, Wang L, Riebe M, Tung HH, Prud'homme RK. 2009. Formulation and stability of ltraconazole and odanacatib nanoparticles: Governing physical parameters. Mol Pharm 6:1118–1124.
33. Zhu ZX, Anacker JL, Ji SX, Hoye TR, Macosko CW, Prud'homme RK. 2007. Formation of block copolymer-protected nanoparticles via reactive impingement mixing. Langmuir 23:10499–10504.

34. Hartley PG, Bailey AI, Luckham PF, Batts G. 1993. Nonspecific interactions between heparin and poly-L-lysine surfaces. Colloids Surf Physicochem Eng Aspects 77:191–198.
35. Kito M, Takimoto R, Yoshida T, Nagasawa T. 2002. Purification and characterization of an epsilon-poly-L-lysine-degrading enzyme from an epsilon-poly-L-lysine-producing strain of Streptomyces albulus. Arch Microbiol 178:325–330.
36. Obst M, Steinbuchel A. 2004. Microbial degradation of poly(-amino acid)s. Biomacromolecules 5:1166–1176.
37. Saimura M, Takehara M, Mizukami S, Kataoka K, Hirohara H. 2008. Biosynthesis of nearly monodispersed poly(epsilon-L-lysine) in streptomyces species. Biotechnol Lett 30:377–385.
38. Hiraki J, Ichikawa T, Ninomiya S, Seki H, Uohama K, Kimura S, Yanagimoto Y, Barnett JW. 2003. Use of ADME studies to confirm the safety of epsilon-polylysine as a preservative in food. Regul Toxicol Pharmacol 37:328–340.
39. El-Aneed A. 2004. An overview of current delivery systems in cancer gene therapy. J Control Release 94:1–14.
40. Godbey WT, Wu KK, Mikos AG. 1999. Poly(ethylenimine) and its role in gene delivery. J Control Release 60:149–160.
41. von Harpe A, Petersen H, Li YX, Kissel T. 2000. Characterization of commercially available and synthesized polyethylenimines for gene delivery. J Control Release 69:309–322.
42. Brissault B, Kichler A, Guis C, Leborgne C, Danos O, Cheradame H. 2003. Synthesis of linear polyethylenimine derivatives for DNA transfection. Bioconjugate Chem 14:581–587.
43. Weyts KF, Goethals EJ. 1988. New synthesis of linear polyethyleneimine. Polym Bull 19:13–19.
44. Alonso JM, Prego C, Garcia-Fuentes M. 2007. Polysaccharide-based nanoparticles as carriers for drug and vaccine delivery. In: Domb AJ, Tabata Y, Ravi Kumar MNV, Farber S, editors. Nanoparticles for pharmaceutical applications. California: American Scientific Publishers.
45. Brunel F, Veron L, David L, Domard A, Delair T. 2008. A novel synthesis of chitosan nanoparticles in reverse emulsion. Langmuir 24:11370–11377.
46. Hunter AC. 2006. Molecular hurdles in polyfectin design and mechanistic background to polycation induced cytotoxicity. Adv Drug Deliv Rev 58:1523–1531.
47. Lehr CM, Bouwstra JA, Schacht EH, Junginger HE. 1992. In vitro evaluation of mucoadhesive properties of chitosan and some other natural polymers. Int J Pharm 78:43–48.
48. Jakes J. 1988. Testing of the constrained regularization method of inverting Laplace transform on simulated very wide quasielastic light-scattering auto-correlation functions. Czech J Phys 38:1305–1316.
49. Jakes J. 1995. Regularized positive exponential sum (REPES) program—A way of inverting laplace transform data obtained by dynamic light scattering. Collect Czech Chem Commun 60: 1781–1797.
50. Cho JY, Heuzey MC, Begin A, Carreau PJ. 2006. Viscoelastic properties of chitosan solutions: Effect of concentration and ionic strength. J Food Eng 74:500–515.
51. Talmon Y. 1999. Cryogenic temperature transmission electron microscopy in the study of surfactant systems. Surfactant Sci Ser 83:147–178.
52. Cheng JC, Olsen MG, Fox RO. 2009. A microscale multi-inlet vortex nanoprecipitation reactor: Turbulence measurement and simulation. Appl Phys Lett 94:3.
53. Matteucci ME, Hotze MA, Johnston KP, Williams RO. 2006. Drug nanoparticles by antisolvent precipitation: Mixing energy versus surfactant stabilization. Langmuir 22:8951–8959.
54. Mordi RC, Walton JC, Burton GW, Hughes L, Ingold KU, Lindsay DA, Moffatt DJ. 1993. Oxidative-degradation of beta-carotene and beta-apo-8'-carotenal. Tetrahedron 49:911–928.
55. Choi HS, Yamamoto K, Ooya T, Yui N. 2005. Synthesis of poly(epsilon-lysine)-grafted dextrans and their pH- and thermosensitive hydrogelation with cyclodextrins. ChemPhysChem 6:1081–1086.
56. Huh KM, Tomita H, Ooya T, Lee WK, Sasaki S, Yui N. 2002. pH dependence of inclusion complexation between cationic poly(epsilon-lysine) and alpha-cyclodextrin. Macromolecules 35:3775–3777.
57. Oku N, Aoyama K, Shibamoto S, Ito F, Gondo H, Nango M. 1987. pH-dependent fusion of lipid vesicles induced by proton-sensitive polymer. Chem Lett 16:1699–1702.
58. Tsuchida E, Nishikawa H. 1976. Effect of a polymer ligand on complexation kinetics of copper(II)-polyethyleneimine. J Polym Sci Part A: Polym Chem 14:1557–1560.
59. Lindquist GM, Stratton RA. 1976. Role of polyelectrolyte charge-density and molecular-weight on adsorption and flocculation of colloidal silica with polyethyleneimine. J Colloid Interface Sci 55:45–59.
60. Claesson PM, Ninham BW. 1992. pH-dependent interactions between adsorbed chitosan layers. Langmuir 8:1406–1412.
61. Hancock BC, Parks M. 2000. What is the true solubility advantage for amorphous pharmaceuticals? Pharm Res 17:397–404.
62. Auweter H, Haberkorn H, Heckmann W, Horn D, Luddecke E, Rieger J, Weiss H. 1999. Supramolecular structure of precipitated nanosize beta-carotene particles. Angew Chem Int Ed 38:2188–2191.